







Analysis of a Complex-Valued Droop Method for Complete Steady-State Frequency Compensation Using dq -Decomposition

Carlos Gómez-Aleixandre , Member, IEEE, Ángel Navarro-Rodríguez , Member, IEEE, Cristian Blanco , Senior Member, IEEE, Geber Villa , Andrés Suárez , and Pablo García , Senior Member, IEEE

Abstract—This article proposes a novel droop technique for AC microgrids with no frequency deviation in steady-state. This droop implementation replaces the conventional $P/f + Q/V$ and $P/V + Q/f$ for inductive and resistive lines respectively by a S/V_{dq} complex-valued droop in which the coupling terms that appear when the line is not purely inductive/resistive are considered. The proposed droop departs from the conventional approach by considering the dq -decomposition instead of calculating P and Q expressions derived from the voltage polar equation, which requires sine and cosine terms. This allows to create a droop combining both voltage components versus P and Q , without requiring small-signal simplification of the trigonometric functions ($\sin \delta \approx \delta$ and $\cos \delta \approx 1$) and taking into account the coupling terms. In that way, the designed droop is valid for any R/X ratio. The discussion is supported with small-signal analysis and hardware-in-the-loop validation.

Index Terms—Distributed power generation, microgrids, power flow control, power distribution control, reactive power control, voltage control.

I. INTRODUCTION

DROOP control is a widely used and a well-known solution for power sharing without requiring communication among converters. There are two main variants depending on the line impedance: $P/f + Q/V$ and $P/V + Q/f$ for

Manuscript received 22 January 2023; revised 26 May 2023; accepted 19 July 2023. Date of publication 1 August 2023; date of current version 22 November 2023. Paper 2022-IACC-1137.R1, presented at the 2021 IEEE Energy Conversion Congress and Exposition, Vancouver, BC Canada, October 10-14, and approved for publication in the IEEE TRANSACTIONS ON INDUSTRY APPLICATIONS by the Industrial Automation and Control Committee of the IEEE Industry Applications Society [DOI: 10.1109/ECCE47101.2021.9595227]. This work was supported in part by the predoctoral grants program FPU for the Formation in University Teaching of Spain MECD under Grant FPU16/05313, in part by the European Union's H2020 Research and Innovation Programme under Grant 864459 (UE-19-TALENT-864459), in part by the Spanish Ministry of Innovation and Science funded by MCIN/AEI/10.13039/501100011033 under Grants MCI-20-PID2019-111051RB-I00 and MCINN-22-TED2021-129796B-C21, in part by the European Union NextGenerationEU/PRTR, and in part by the Principality of Asturias, FICYT, FEDER Funds under Grant SV-PA-21-AYUD/2021/57546. (Corresponding author: Carlos Gómez-Aleixandre.)

The authors are with the Department of Electrical, Electronics, Computers, and Systems Engineering, University of Oviedo, 33204 Gijón, Spain (e-mail: gomezcarlos@uniovi.es; navarroangel@uniovi.es; blancocristian@uniovi.es; villageber@uniovi.es; suarezandres@uniovi.es; garciafpablo@uniovi.es).

Color versions of one or more figures in this article are available at <https://doi.org/10.1109/TIA.2023.3300259>.

Digital Object Identifier 10.1109/TIA.2023.3300259

inductive and resistive lines respectively [1]. In both cases, the following considerations apply: 1) lines are assumed to be purely inductive/resistive, neglecting the orthogonal impedance term; 2) phase angle difference, δ , between voltages is small, thus allowing to approximate $\sin \delta \approx \delta$ and $\cos \delta \approx 1$; and 3) frequency and voltage have a steady-state deviation with respect to the rated conditions.

Neglecting the resistive/inductive part can worsen the operation when R/X ratio is close to 1, thus the coupling term effect becoming significant. Virtual impedance can be included to increase the resistive/inductive component of the line impedance [2], [3], but this would cause some unwanted side effects, like the degradation of voltage regulation due to steady-state voltage drop across the virtual impedance [4].

Some solutions can be found in the literature that consider the coupling terms. In [5], [6], an orthogonal linear rotational transformation matrix (obtained from the impedance phase angle) is used to rotate P and Q so that the coupling terms are avoided. In [7], [8], the coupling terms are compensated. This is done by introducing in the expression for each droop output (voltage magnitude and frequency) a term to compensate the effect of the deviation of the other output with respect to the nominal value.

Other solutions are found in the literature using angle instead of frequency as one of the droop outputs [8], [9], [10], [11], thus eliminating frequency deviation. In this article, the dq -decomposition is considered instead. This avoids the trigonometric function simplification considered when using the voltage polar expression, thus obtaining a compact formulation using complex numbers.

Solutions based in the dq -decomposition have been already proposed in [12]. However, it includes a PLL mechanism which produces a frequency deviation in steady state. In [13], [14], a PLL-less solution is proposed, in which frequency variations only occurs during transients. The proposal has only been validated by simulations. Besides that, the impedance phase angle is not considered for the droop application in none of them, including the mentioned alternatives based in angle droop [8], [9], [10], [11].

The proposed alternative in this article has no frequency deviation in steady-state; considers the effect of impedance phase angle for the droop design, including an analysis of

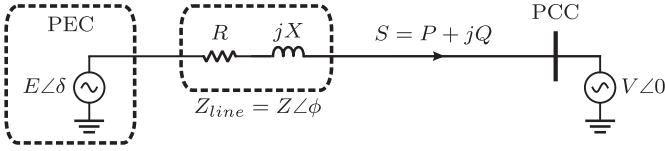


Fig. 1. Power flow diagram in a line impedance connecting a power electronic converter (PEC) to the grid.

mismatches for this angle estimation, and is validated with a Hardware-in-the-Loop (HIL) system. A secondary control is included, based on an adaptation of the proposal in [15].

This article continues the study presented in [16]. The updated version extends the research in the following directions: 1) evaluation of the proposed control with HIL, 2) small-signal model analysis of the proposed control compared with conventional $P/f + Q/V$ or $P/V + Q/f$ droops, 3) secondary control proposal for the complex-valued droop, 4) negative values of R/X ratio are considered, for inverters with output impedance dominated by a capacitive virtual impedance [17]. It will be shown that the proposed droop is valid for this scenario. This is also the case for $P/V + Q/f$ droop, referred to as universal droop in [18]. Conversely, conventional $P/f + Q/V$ droop is not suitable for the capacitive impedance operation.

This article is organized as follows. In Section II, the proposed droop control is explained. In Section III, the voltage deviation caused by the proposed droop is compared with the $P/f + Q/V$ and $P/V + Q/f$ alternatives. In Section IV, the grid used for the study is presented. In Section V, the performance and stability are analyzed, being compared with alternative conventional droops by using a small-signal model approximation. In Section VI, a secondary control for the proposed droop is presented. Section VII shows the HIL results based on a Typhoon platform. Firstly, the proposed droop is compared with $P/f + Q/V$ and $P/V + Q/f$ approaches, assuming perfect knowledge of impedance phase angle for orthogonal linear rotational transformation matrix. Then, the effect of mismatches in the estimation of the impedance phase angle is analyzed by different scenarios with significant estimation errors. Section VIII presents an analysis of the steady-state power sharing accuracy of the proposed droop. This analysis is validated by comparing with the HIL results in Section VII but allows to study the whole range of possible load power factors. Finally, Section IX presents the conclusions.

II. PROPOSED DROOP CONTROL

A diagram for the power flow in a generic line with arbitrary impedance is shown in Fig. 1. Conventional $P/f + Q/V$ and $P/V + Q/f$ droops are obtained from the same diagram assuming $R \approx 0$ and $X \approx 0$, respectively.

In this article, polar expressions for voltage and impedance are replaced with their equivalent rectangular equations in the synchronous dq -reference frame and complex numbers are used for the calculations.

For the following derivations, steady-state situation is considered. However, the outputs of the droop are used as references for the instantaneous values of the voltage components.

Apparent power calculation is shown in (1), being S , P and Q apparent, active and reactive power flowing to the point of common coupling (PCC) from the power electronic converter (PEC); V_{dq} the voltage vector at the PCC and $\overline{I_{dq}}$ the conjugate of the line current vector. For this article, power invariant transformation is considered ($k = 1$). Still the following discussion is equivalent for the magnitude invariant transformation, leading to equivalent expressions.

$$S = P + jQ = kV_{dq}\overline{I_{dq}} \xrightarrow{k=1} S = P + jQ = V_{dq}\overline{I_{dq}} \quad (1)$$

The conjugate of the current can be obtained as shown in (2) from the converter output voltage, E_{dq} , the voltage at the PCC, V_{dq} , and the impedance of the line connecting them. The voltage expression at the PCC can be simplified as $V_{dq} = V_d = V$, since the d -axis is used as the phase reference.

$$\overline{I_{dq}} = \overline{\left(\frac{E_{dq} - V_{dq}}{Z_{line}}\right)} = \frac{\overline{E_d + jE_q - V}}{\overline{R + jX}} = \frac{E_d - V - jE_q}{R - jX} \quad (2)$$

Substituting (2) in (1), (3) is obtained.

$$S = V \frac{E_d - V - jE_q}{R - jX} = V \frac{(E_d - V - jE_q)(R + jX)}{(R - jX)(R + jX)} \quad (3)$$

Taking into account that $(R - jX)(R + jX) = Z^2$, the expression shown in (4) is obtained, being Z the modulus of the complex impedance.

$$S = \frac{V}{Z^2}(E_d - V - jE_q)(R + jX) \quad (4)$$

Splitting (4) into real and imaginary components, the expressions for active and reactive power are obtained, as shown in (5a) and (5b).

$$P = \frac{V}{Z^2}(E_d R + E_q X - V R) \quad (5a)$$

$$Q = \frac{V}{Z^2}(E_d X - E_q R - V X) \quad (5b)$$

From (5a) and (5b), $P/f + Q/V$ and $P/V + Q/f$ droops can be obtained by substituting $E_d = E \cos \delta \approx E$ and $E_q = E \sin \delta \approx E\delta$ and considering $R \approx 0$ or $X \approx 0$ respectively, as shown in (6) and (7) [1].

$$P \approx \frac{V}{X} E \delta \rightarrow \omega - \omega_0 = -m_\omega (P - P_0) \quad (6a)$$

$$Q \approx \frac{V}{X} (E - V) \rightarrow E - E_0 = -m_V (Q - Q_0) \quad (6b)$$

$$P \approx \frac{V}{R} (E - V) \rightarrow E - E_0 = -m_V (P - P_0) \quad (7a)$$

$$Q \approx -\frac{V}{R} E \delta \rightarrow \omega - \omega_0 = m_\omega (Q - Q_0) \quad (7b)$$

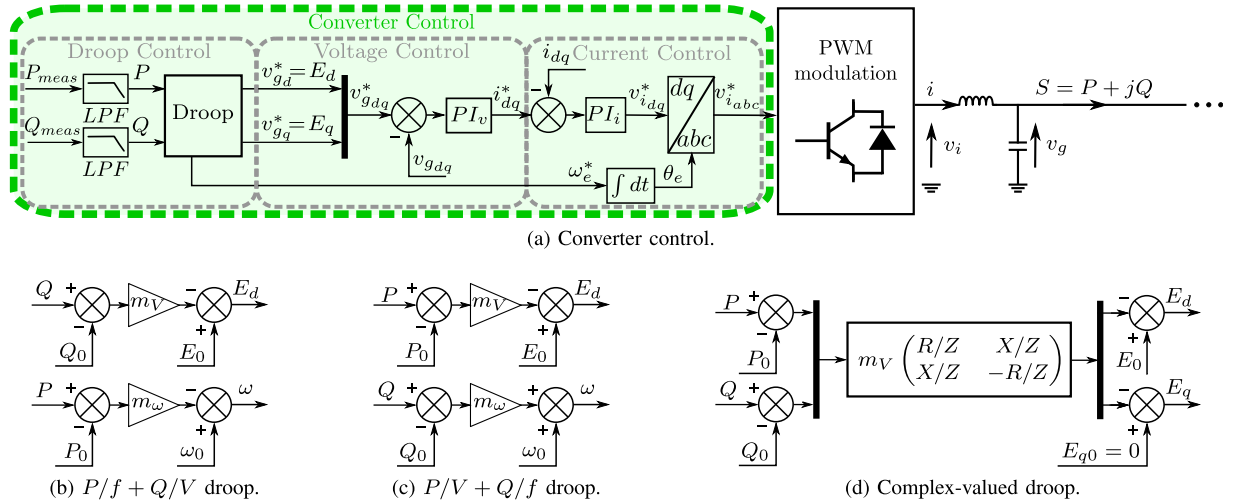


Fig. 2. Control scheme including the different droop control methods. For $P/f + Q/V$ and $P/V + Q/f$ droops, E_q reference is set to 0 and for complex-valued droop ω reference is set to 100π rad/s (50 Hz). For this paper $P_0 = Q_0 = 0$, except when these values are calculated by the secondary control.

Equations (5a) and (5b) can be expressed in matrix form as shown in (8).

$$\begin{pmatrix} P \\ Q \end{pmatrix} = \frac{V}{Z^2} \left[\begin{pmatrix} R & X \\ X & -R \end{pmatrix} \begin{pmatrix} E_d \\ E_q \end{pmatrix} - \begin{pmatrix} R \\ X \end{pmatrix} V \right] \quad (8)$$

From (8), applying a droop coefficient, m_V , to relate E_d and E_q variations with both P and Q , the proposed droop formula shown in (9) is obtained similarly to $P/f + Q/V$ and $P/V + Q/f$ in (6) and (7).

$$\begin{pmatrix} E_d - E_{d0} \\ E_q - E_{q0} \end{pmatrix} = -m_V \begin{pmatrix} R/Z & X/Z \\ X/Z & -R/Z \end{pmatrix} \begin{pmatrix} P - P_0 \\ Q - Q_0 \end{pmatrix} \quad (9)$$

This complex-valued droop, obtained from the dq -decomposition, takes into account the coupling between P and Q . It only requires knowledge on the line R/X ratio and, by applying the droop to both voltage components instead of magnitude and frequency, enables no frequency deviation in steady-state.

Considering the analyzed droop alternatives, the complete converter control scheme is shown in Fig. 2, together with the different droop controllers. Details about cross-coupling and feed-forward terms, normalization and nonlinear compensation can be seen in [19].

III. COMPLEX-VALUED DROOP VOLTAGE DEVIATION IN STEADY-STATE

Applying a droop related to voltage components will cause a voltage deviation with respect to nominal value in the same way $P/f + Q/V$ and $P/V + Q/f$ alternatives have deviations with respect to frequency and voltage. In our proposal, since both components, E_d and E_q , are involved in the droop calculation, the combined effect of both components shall be analyzed to assess if the impact in the voltage deviation is increased.

Considering $\Delta S = \Delta P + j\Delta Q = (P - P_0) + j(Q - Q_0)$ and $\Delta E = \Delta E_d + j\Delta E_q = (E_d - E_{d0}) + j(E_q - E_{q0})$, (9)

can be rewritten as (10).

$$\begin{pmatrix} \Delta E_d \\ \Delta E_q \end{pmatrix} = -m_V \begin{pmatrix} R/Z & X/Z \\ X/Z & -R/Z \end{pmatrix} \begin{pmatrix} \Delta P \\ \Delta Q \end{pmatrix} \quad (10)$$

For this demonstration, the PEC is considered to be producing an apparent power S , expressed as a complex number $S = P + jQ = |S|\angle\alpha$. For the results in this article $P_0 = Q_0 = 0$, resulting in $\Delta S = S$. As shown in Fig. 2(d), $E_{q0} = 0$ and $E_{d0} = E_0$, that for simplicity will be expressed in per unit as $E_{d0} = 1$ pu. Expressing the matrix (10) in complex number form, (11) is obtained, where $(R/Z + jX/Z)$ is a complex number with modulus 1 and angle ϕ and $(P - jQ)$ is the conjugate of the apparent power.

$$\Delta E = -m_V (R/Z + jX/Z) (P - jQ) \quad (11)$$

Expressing $(R/Z + jX/Z)$ and $(P - jQ)$ in its polar expression and doing the product, expression (11) can be rewritten as shown in (12), being β the difference between line impedance phase angle and apparent power angle ($\phi - \alpha$).

$$\Delta E = -m_V |S| (\cos \beta + j \sin \beta) \quad (12)$$

From (12), and taking into account that $E_{d0} = 1$ pu, the voltage amplitude is obtained using (13).

$$|E| = \sqrt{(1 - m_V |S| \cos \beta)^2 + (m_V |S| \sin \beta)^2} \quad (13)$$

Taking into account $\cos^2 \beta + \sin^2 \beta = 1$, the deviation in the voltage amplitude due to the proposed droop method with respect to nominal value (1 pu) is obtained by (14).

$$\Delta |E| = \sqrt{1 - 2m_V |S| \cos \beta + m_V^2 |S|^2} - 1 \quad (14)$$

It is important to remark here, that for all the demonstration before, the values used for impedance phase angle are not the real ones, but the ones assumed by the droop control. This means that in case the estimation of the angle is not correct, the one involved in the voltage deviation effect is the estimated one (from now on ϕ_{est}).

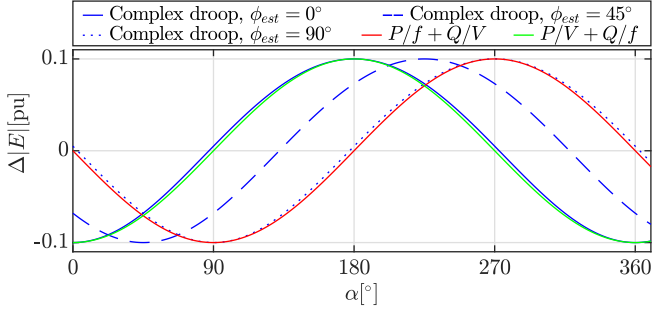


Fig. 3. Variation of voltage amplitude output for different values of α (apparent power angle), with $m_V|S| = 0.1$ pu.

The maximum deviation in the voltage amplitude is obtained for $\beta = 0^\circ$ and $\beta = 180^\circ$, as shown in (15a) and (15b) respectively.

$$\Delta|E| = \sqrt{1 - 2m_V|S| + m_V^2|S|^2} - 1 = -m_V|S| \quad (15a)$$

$$\Delta|E| = \sqrt{1 + 2m_V|S| + m_V^2|S|^2} - 1 = m_V|S| \quad (15b)$$

Where m_V is expressed in per unit value. This means that the maximum value for the voltage amplitude deviation is obtained when the line impedance and the apparent power have opposite phases while the minimum occurs when they are aligned. In both cases, the deviation from nominal value is $m_V|S|$ in absolute value.

Taking this into account, it can be concluded that the range for the voltage amplitude deviation obtained from the proposed droop control for $|S| \leq S_n$ is $(-m_V, m_V)$, equivalent to the $P/f + Q/V$ and $P/V + Q/f$ droops for a variation of P or Q in the range of $(-S_n, S_n)$.

In the case of $P/f + Q/V$ and $P/V + Q/f$ droops, voltage amplitude is only a function of active/reactive power with a linear relationship. Meanwhile, in the proposed complex-valued droop, it depends on both apparent power magnitude and phase difference with respect to the line impedance phase angle. This relationship, for a fix value of $|S|$, is shown in Fig. 3, with the deviation in the output voltage for different values of the apparent power angle (α). The curve for $P/f + Q/V$ and $P/V + Q/f$ is a sinusoidal waveform, since for a fixed value of $|S|$, the relationship of the voltage variation with respect to the angle is $\Delta|E| = -m_V Q = -m_V|S| \sin(\alpha)$ and $\Delta|E| = -m_V P = -m_V|S| \cos(\alpha)$ respectively.

Since the dependence of the voltage deviation with respect to the angle shown in (14) is for $\beta = \phi_{est} - \alpha$, different values of ϕ_{est} result in a horizontal displacement of the corresponding $\Delta|E|$ vs α curve. When $\phi_{est} = 0^\circ$, the corresponding curve (continuous blue) is very similar to the one corresponding to $P/V + Q/f$ droop (continuous green), meanwhile when $\phi_{est} = 90^\circ$ the corresponding curve (dotted blue) is very similar to the one corresponding to $P/f + Q/V$ droop (continuous red). In all the cases, the maximum voltage deviation is $m_V|S|$.

In Fig. 4, the variation of the voltage amplitude with respect to the apparent power is shown for different values of angle β . Taking into account that β was defined as $\phi_{est} - \alpha$

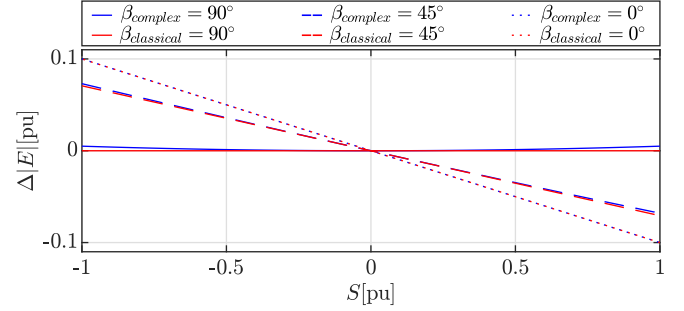


Fig. 4. Variation of the voltage amplitude output for different values of S , with $m_V = 0.1$ pu. Blue lines correspond to the proposed complex droop and red lines to the conventional $P/f + Q/V$ and $P/V + Q/f$ alternatives. For $\beta = 0^\circ$, the three droops produce the same variation (red and blue dotted lines coincide).

for the proposed droop, it can be defined in a similar way for $P/f + Q/V$ and $P/V + Q/f$ considering $\phi_{est} = 90^\circ$ and $\phi_{est} = 0^\circ$ respectively. With this notation, $\beta = 0^\circ$ implies apparent power to be purely reactive for $P/f + Q/V$ droop and active for $P/V + Q/f$, producing the maximum voltage deviation. In Fig. 4, S is considered as a real number, having the apparent power the direction of β and being positive for power production and negative for consumption.

A. Droop Coefficient Selection

Taking into account that the proposed droop produces a voltage output variation range equal to the one obtained for $P/f + Q/V$ and $P/V + Q/f$ droops, the starting point for selection of the droop coefficient can be done taking into account the maximum variation of the voltage output.

For this article, a maximum voltage deviation of 5% is used for droop coefficient selection, based on a tradeoff between power sharing accuracy and voltage regulation [20]. Due to the similar effect in voltage deviation produced by the conventional droops ($P/f + Q/V$ and $P/V + Q/f$) and the proposed complex-valued alternative, the same value for the coefficient is used for the three cases and using the same name for this coefficient (m_V).

IV. CASE STUDY

The grid used as case study is shown in Fig. 5, where PEC_1 and PEC_2 are droop-controlled power electronic converters connected in node 1 and 3 respectively. Constant impedance loads (R-L series circuit) are connected in node 2 (CIL₁) and 4 (CIL₂) and a converter connected to distributed energy storage system (dESS) is connected to node 5, behaving as a constant power load (CPL), with 500 Hz current control bandwidth.

The used grid is one of the ac feeders from the microgrid shown in [21]. For demonstration purposes, both converters are considered to be equal with a rated power of 30 kVA. Converter parameters are shown in Table I.

To compare the performance of the proposed complex-valued droop with respect to $P/f + Q/V$ and $P/V + Q/f$ droops, the

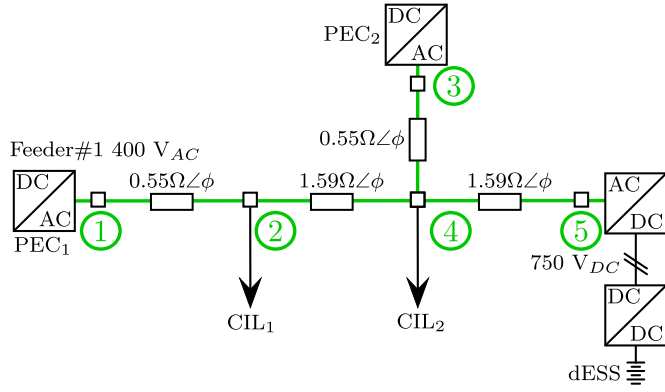


Fig. 5. Grid used for validation. Impedance phase angle (ϕ) varies for different scenarios.

TABLE I
CONVERTER PARAMETERS

S_n	30 kVA	PI _i : Bandwidth	500 Hz
R_{filter}	0.1 Ω	PI _v : Bandwidth	50 Hz
L_{filter}	1.35 mH	Droop: m_V	0.05 pu
C_{filter}	980 μ F	Droop: m_ω	0.02 pu

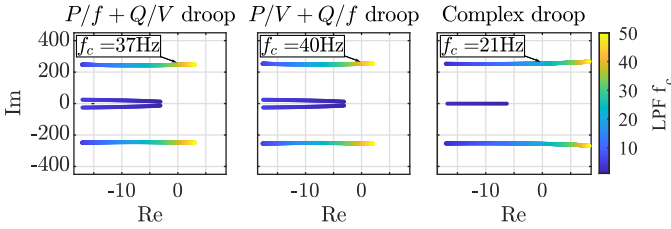


Fig. 6. Dominant eigenvalues for each type of droop considering inductive lines in function of the LPF cutoff frequency (f_c) for the power measurement. The cutoff frequency at which it becomes unstable is shown for each droop.

impedance phase angle (ϕ) is varied. Three different angles (0° , 45° and 90°) are considered in the HIL results.

V. SMALL-SIGNAL ANALYSIS

For analyzing the stability of the proposed complex droop, a small-signal model analysis is presented and compared to the conventional droops. A sensitivity analysis for parameter variation is performed for all of them, varying the power measurement LPF cutoff frequency, f_c . All the other parameters are the ones used for HIL, shown in Section IV. In Fig. 6, the dominant eigenvalues for each case are shown, together with the values of f_c at which it becomes unstable. For this analysis, an inductive line was considered, since it was found to be the most critical condition (the resistive and resistive-inductive case are stable for values greater than the limit f_c shown in Fig. 6).

The proposed droop becomes unstable for $f_c > 21$ Hz, meanwhile the conventional droops become unstable for $f_c > 37$ Hz and $f_c > 40$ Hz respectively. However, even if lower cutoff frequency is required, the transient response is really similar for the three types of droops, with very close dominant eigenvalues

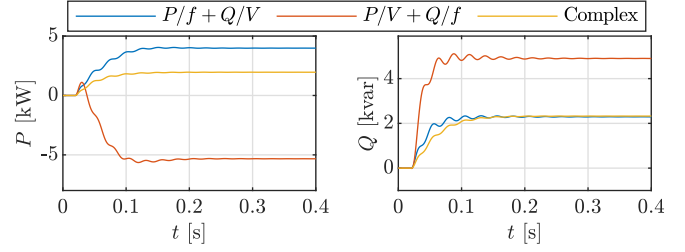


Fig. 7. Step responses for each type of droop with inductive lines.

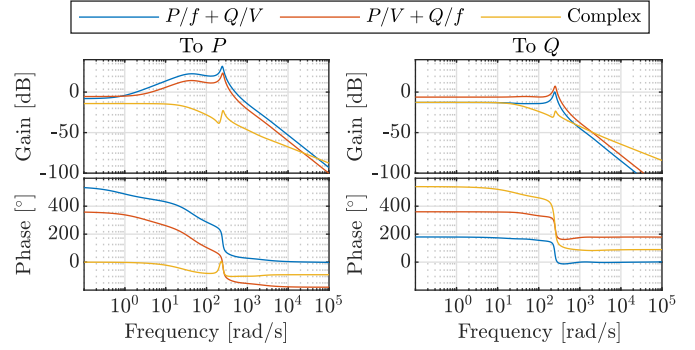


Fig. 8. Bode diagram for each type of droop with inductive lines.

(-14.4 ± 246.1 , -15.2 ± 251.9 and -14.7 ± 252.4). This can be seen in Fig. 7, where f_c is 10 Hz, 10 Hz and 5 Hz for $P/f + Q/V$, $P/V + Q/f$ and proposed complex droop. Fig. 8 shows the corresponding bode diagram, with a resonance peak that explains the oscillations in the step response. In Section VII, these results are extended to consider different line configurations. The two steps represent a connection in node 4 of a CIL of 10 kW and 10 kvar respectively, showing the active and reactive power output at PEC₁. Only one PEC output is shown, since the dynamics of both of them are similar, being the obtained steady-state value the main difference. Regarding the steady-state, it is clearly worse in the $P/V + Q/f$ droop because of the inductive case. A more extensive discussion regarding the general steady-state behavior is presented in Section VIII.

VI. SECONDARY CONTROL

Secondary control is based in an adaptation of the proposal in [15]. The algorithm, shown in Fig. 9, consists of calculating the power flow solution for the grid and calculate the offset power (P_0 and Q_0) so that the droop characteristic contains the point obtained from the power flow. This algorithm is executed in a central controller which sends the offset power to each PEC. The power flow can be solved using any criteria for power sharing among the converters, being a flexible solution. For this article, equal power sharing among the converters is chosen. Besides that, one of the nodes is determined to have 1 pu voltage, being the focus of the secondary control and considered as the area voltage whose level must be restored. PEC₁ output is used for the present paper.

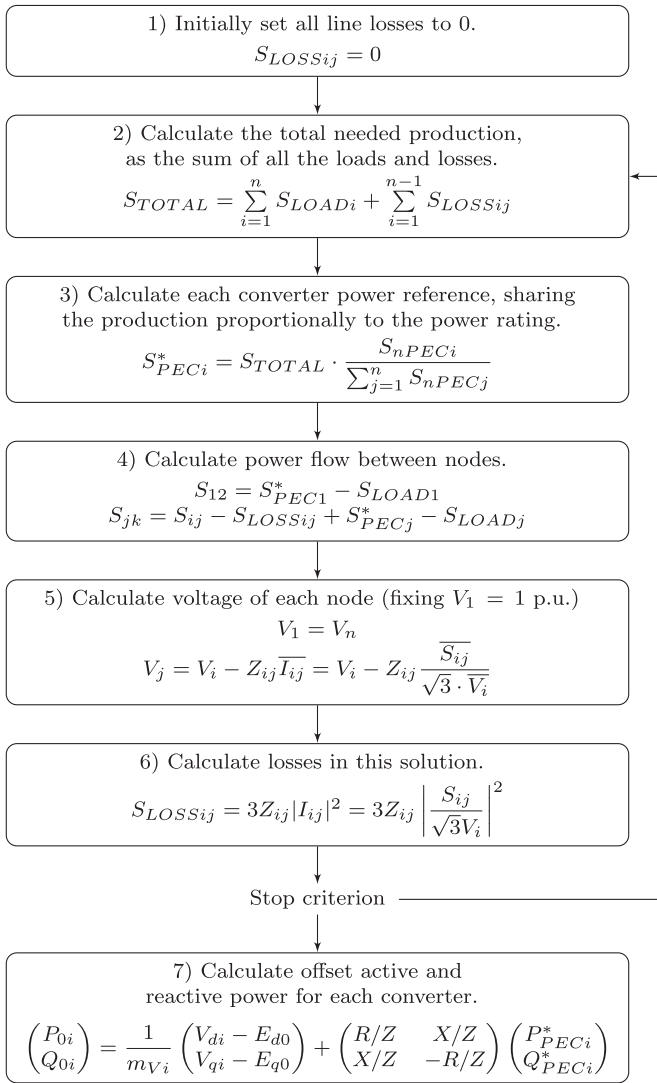


Fig. 9. Flowchart for secondary control. i, j and k denote any three consecutive nodes. For obtaining a more compact expression, active and reactive power equations are presented in its complex form, so they are joint into one equation with $S = P + iQ$, using also $Z = R + iX$ and $V = V_d + V_q \cdot \bar{x}$ indicates conjugate of a complex vector.

Starting assuming no losses (step 1), an iteration for the calculation of the power flow is performed (step 2 to 6). After one iteration of the power flow with the desired power sharing is performed, a stop criterion is used for checking the convergence of the algorithm. This criterion can be a given number of iterations or a tolerance (comparing the result of one iteration with the previous one until it is lower than a given threshold). As analyzed in [15], the performance of the secondary control is sufficiently good even for the first iteration of the algorithm, so only one iteration is done for this article. The possibility of performing more iterations is considered in Fig. 9 for being more general.

After finishing the power flow calculations, each of the droop controlled converters voltage and power outputs are known. The active and reactive power offset (P_0 and Q_0) are obtained (step 7) so that the droop equation, (9), contains the values from

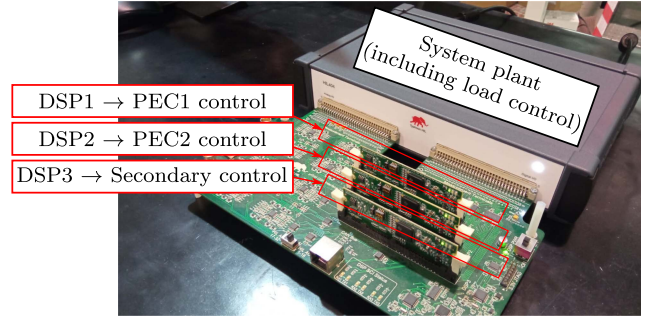


Fig. 10. Typhoon HIL404 Hardware-in-the-Loop setup. The HIL is composed by 1 Typhoon HIL404, 1 HIL uGrid DSP Typhoon Interface and 3 TMS320F28335 TI control cards. DSP3 sends the secondary control references to DSP1 and DSP2 by CAN bus.

the power flow solution with the chosen criteria (for this article, equal active and reactive power sharing between PEC_1 and PEC_2 and $V_1 = 1$ pu).

VII. HARDWARE-IN-THE-LOOP RESULTS

The proposed droop control has been validated by using a HIL setup. The HIL setup, shown in Fig. 10, is a Typhoon HIL404. The HIL time step is $1 \mu s$, the sampling time of the converters control is $100 \mu s$ and their switching frequency is 10 kHz. The data shown in this article has been captured with a rate of 100 kS/s. The results are presented filtered for a better visualization (10 Hz low-pass filter), although THD results and three-phase voltages and currents are shown too.

The HIL results are divided in two main parts. In the first one, the proposed droop is compared with the conventional $P/f + Q/V$ and $P/V + Q/f$. Perfect knowledge of the impedance phase angle is assumed. Impedance estimation [22], [23] can be used for online estimation. For the second part, the response of the proposed droop when mismatches occur in the impedance phase angle estimation are analyzed.

A. Comparison of Different Droop Methods

Results for the different impedance phase angles are shown in Fig. 11. Results for the three different alternatives are shown together for a better comparison between the proposed complex-valued droop and the conventional $P/f + Q/V$ and $P/V + Q/f$.

Starting with no load, at $t = 0.1$ s a CIL of 10 kW, 10 kvar is connected in nodes 2 and 4 (Fig. 5). In that situation, the grid is completely symmetric, so both converters have the exact same output. At $t = 0.4$ s another CIL, 10 kW, 10 kvar is connected in node 4. At $t = 1.2$ s the converter in node 5 starts to produce 10 kW, behaving as a CPL.

The proposed droop is able to operate with a good response in all the impedance phase angle range and both for CIL and CPL (bidirectional). Additionally, frequency deviation in steady-state does not appear in the proposed droop, while the variation during the transients is really small. Besides that, it can be seen that the complex-valued droop is able to properly decouple active and reactive power, remaining the reactive power share unchanged

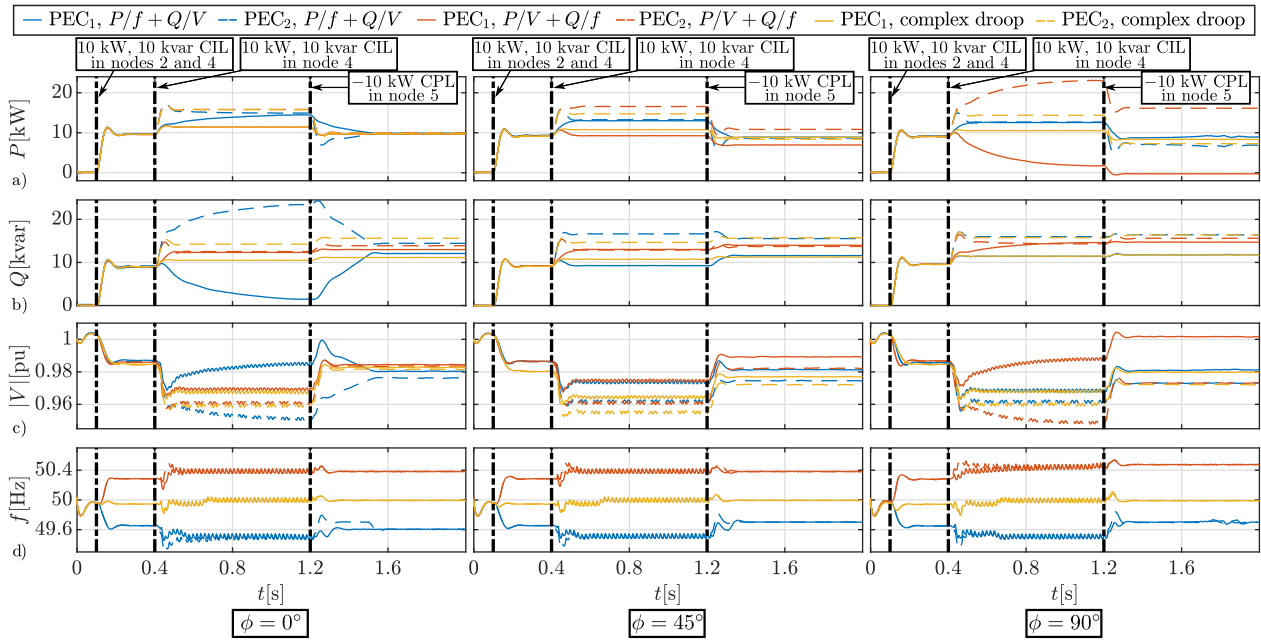


Fig. 11. HIL results for different values of impedance phase angle (ϕ) for the three types of droops: (a) active power production, (b) reactive power productions, (c) output voltage magnitude and (d) frequency.

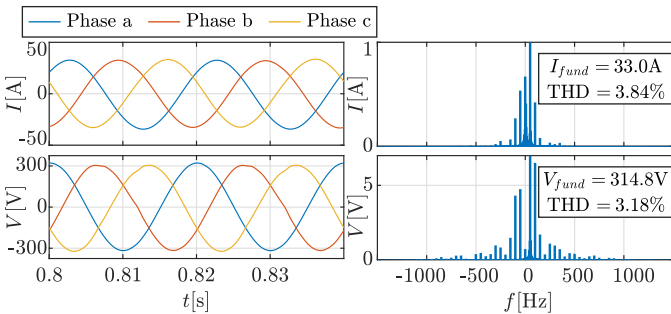


Fig. 12. Phase current and voltage waveforms (left column) for the Hardware-in-the-Loop results with $\phi = 90^\circ$, together with the harmonic decomposition (right column).

when at $t = 1.2$ s an active power step is introduced. As expected from Section V, the transient response of the three droops is very similar, except in the $P/f + Q/V$ ($P/V + Q/f$) droop in the resistive (inductive) case in which its overall performance is clearly worsened. The steady-state performance of the three droops is compared in Section VIII.

As mentioned before, the results shown in Fig. 11 are filtered, but the THD of all the shown scenarios, was measured being all of them below 5%. The THD was measured between $t = 0.8$ s and $t = 1.2$ s, since it is the period with most distortion as can be appreciated in the voltage frequency and magnitude results. Proposed complex droop unfiltered current and voltage of the three phases of PEC₁ are shown in Fig. 12 for the inductive case. This was the case with worse distortion for the proposed droop, with a THD of 3.18% and 3.84% for voltage and current respectively.

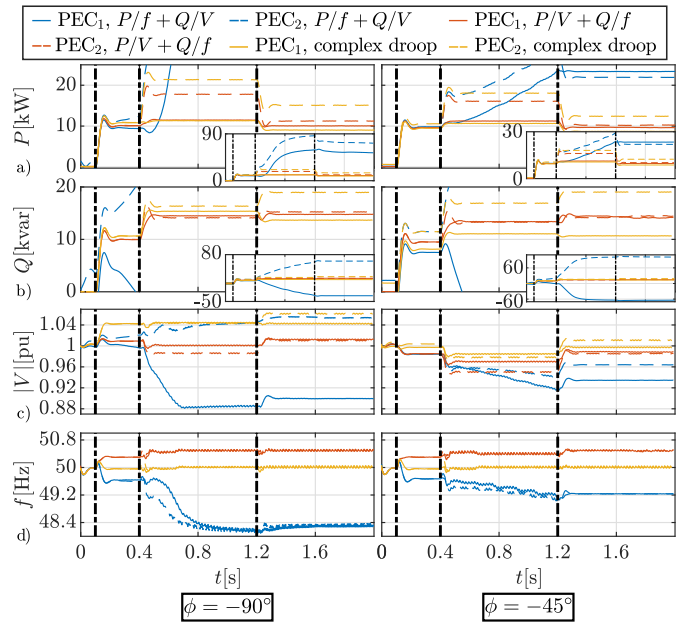


Fig. 13. HIL results for different values of negative impedance phase angle (ϕ) for the three types of droops: (a) active power production, (b) reactive power productions, (c) output voltage magnitude and (d) frequency. Steps (indicated by black dashed vertical lines) are the same of Fig. 11. A zoomed-out view of active and reactive power is included, scaled to the response of the $P/f + Q/V$ droop.

In Fig. 13, negative impedance phase angles are considered for the same scenario shown in Fig. 11. For this scenario, the capacitive impedance is achieved by including a virtual impedance in each converter. This virtual impedance was calculated as 80%

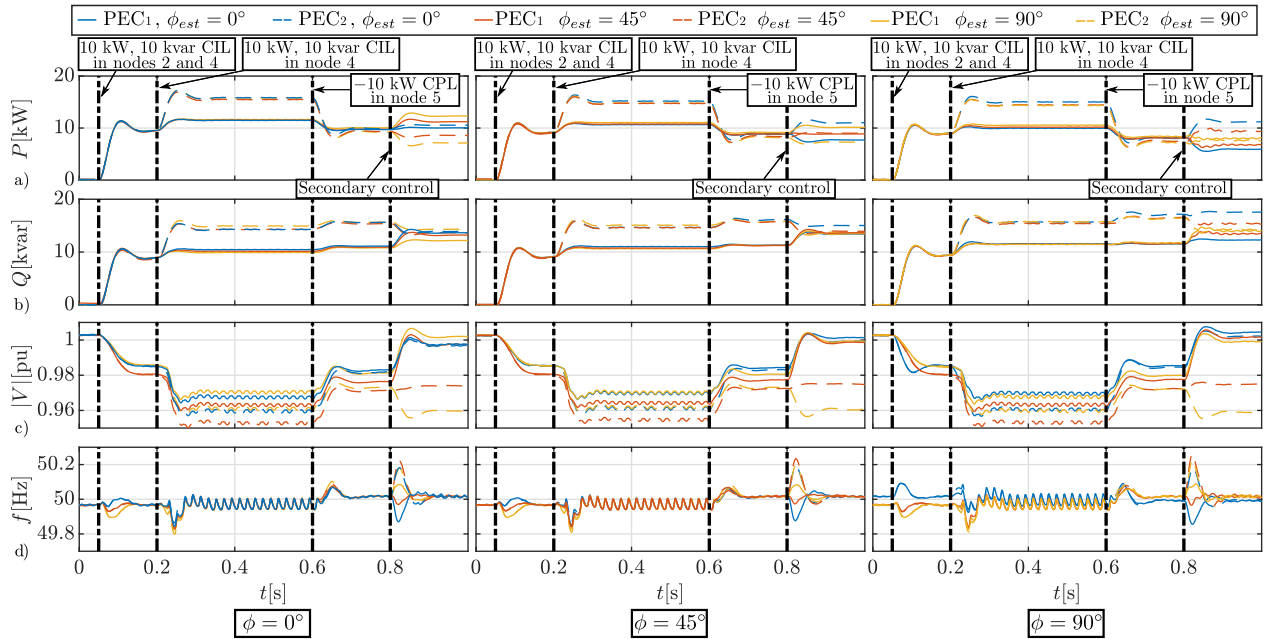


Fig. 14. HIL results for the proposed complex-droop for different values of the impedance phase angle (ϕ) for three values of the estimated impedance phase angle (ϕ_{est}): (a) active power production, (b) reactive power productions, (c) output voltage magnitude and (d) frequency. Lines corresponding to the right estimation are on top of the others to highlight them.

of the coupling impedance shown in Fig. 5, reducing the physical impedance in the same amount in order to achieve similar total output impedance. The rest of the circuit is considered to be purely resistive. It can be seen that the proposed complex droop is suitable for this scenario. $P/V + Q/f$ is valid too, as demonstrated in the analysis in [18], showing the validity of the $P/V + Q/f$ (or universal) droop for the whole range of impedance phase angle. The $P/f + Q/V$ droop is not suitable for this scenario, as can be seen in its really poor performance.

B. Effect of Impedance Phase Angle Estimation Mismatch

In order to analyze the effect of an impedance phase angle estimation mismatch, different scenarios have been analyzed. In Fig. 14, different values of the impedance phase angle are shown with three values for the estimation of the impedance phase angle. The load steps are the same used in Fig. 11 at times $t = 0.05$ s, $t = 0.2$ s and $t = 0.6$ s and adding the application of the secondary control in $t = 0.8$ s. The secondary control results are later explained in Section VII-C.

It can be seen that the proposed control is not very sensitive to the mismatch, as no significant difference in the performance can be seen. The major differences are related to the voltage output amplitude and frequency results. The difference in the frequency is not very significant, taking into account that the deviation from nominal value is small (maximum of 0.26 Hz considering all the scenarios) and recovered quickly. The differences in the voltage amplitude are due to the use of different rotation matrix. As explained in Section III, the deviation in voltage amplitude with respect to nominal value depends on the apparent power magnitude and angle and the angle used for the rotation matrix (ϕ_{est}). It can be seen that the voltage amplitude result is

TABLE II
SECONDARY CONTROL ERROR IN ACTIVE AND REACTIVE POWER SHARING AND VOLTAGE MAGNITUDE

		$\phi = 0^\circ$	$\phi = 45^\circ$	$\phi = 90^\circ$
$\phi_{est} = 0^\circ$	ΔP	0.85%	5.54%	8.79%
	ΔQ	0.40%	2.72%	8.74%
	ΔV_1	0.26%	0.13%	0.45%
$\phi_{est} = 45^\circ$	ΔP	4.39%	0.20%	4.53%
	ΔQ	0.68%	0.44%	2.99%
	ΔV_1	0.25%	0.14%	0.15%
$\phi_{est} = 90^\circ$	ΔP	8.63%	4.70%	0.98%
	ΔQ	3.59%	0.39%	0.14%
	ΔV_1	0.19%	0.06%	0.09%

similar for the same ϕ_{est} , even for different values of the actual line impedance phase angle. The small difference is due to the different power sharing of the PECs when line impedance phase angle changes. The steady-state performance of the three cases is compared in Section VIII.

C. Secondary Control

The secondary control proposed in Section VI is applied in $t = 0.8$ s in Fig. 14. It can be seen that its performance is really accurate when the impedance phase angle estimation is perfect, achieving equal active and reactive power sharing between both converters and 1 pu voltage in PEC₁ output. Table II shows the error of the secondary control, measured in Fig. 14 at $t = 1$ s, with the errors corresponding to the proper estimation highlighted with red. This error is measured as the per unit deviation of the active/reactive power with respect to equal power sharing and voltage in node 1 with respect to rated voltage. The maximum error of all the scenarios is 8.79% for an estimation mismatch of 90° . These extreme cases of

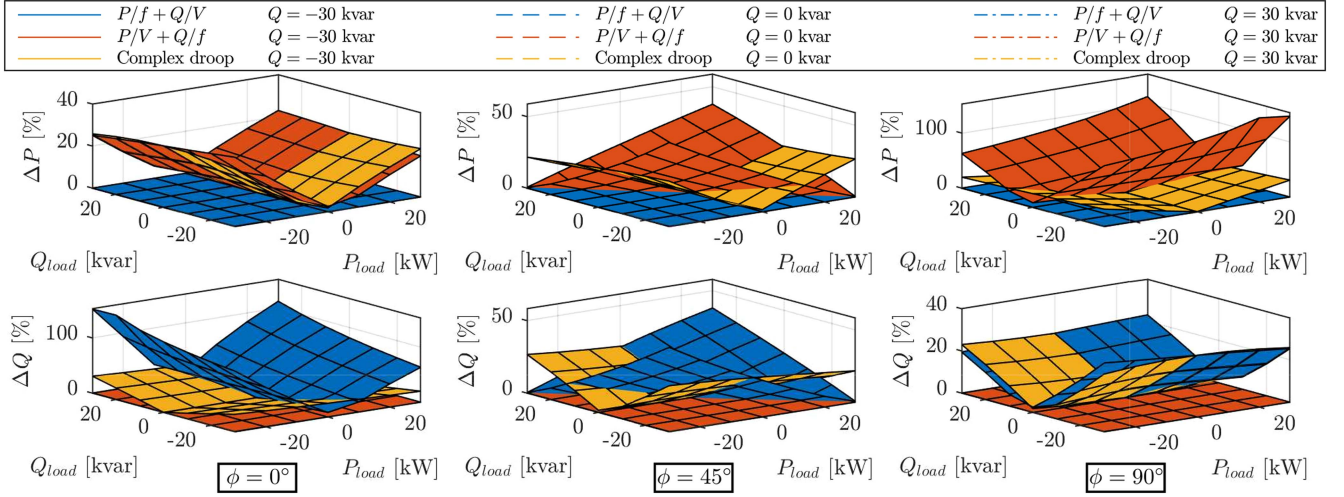


Fig. 15. Steady-state power sharing error comparing the proposed complex droops with the conventional droops. First row: $\Delta P(P_{load}, Q_{load}, \phi)$ with $\phi = 0^\circ$, $\phi = 45^\circ$ and $\phi = 90^\circ$ from left to right column. Second row is equivalent but for ΔQ . These results are summarized in Table III.

estimation mismatch are very unlikely to happen in reality. For 45° estimation mismatch the maximum error is 5.54%, being only 0.98% for perfect estimation.

VIII. POWER SHARING ACCURACY

In this section, an analysis of the power sharing obtained with each droop is performed, in order to quantify the accuracy of the proposed method and compare it with $P/f + Q/V$ and $P/V + Q/f$ droops. The same analysis is performed considering the proposed droop with estimation errors for ϕ .

From the equations used for the small-signal analysis of Section V, the equilibrium point is obtained. In order to check the validity of this equilibrium point calculation, the power sharing of the equilibrium points in Figs. 11 and 14 were calculated, considering only those corresponding to CIL. The HIL results obtained for both active and reactive power output of PEC_1 and PEC_2 immediately before the second and third load connection in Figs. 11 and 14 was calculated, obtaining less than 1.8% error for all the cases shown in Fig. 14 (considering the maximum error of the 4 different variables in the 9 combinations of ϕ and ϕ_{est}). For Fig. 11, the maximum error is 2.88%. This error occurs for the $P/V + Q/f$ droop in the inductive case, since the poor performance of this droop for that scenario causes a significant phase difference between both PECs, resulting in loss of accuracy for the small-signal model (that considers δ to be really small). Apart from that case, the maximum error is never greater than 2%.

For this section, the grid shown in Fig. 5 is used, considering load connections only in node 4. A swept for both active and reactive power between -30 ($-S_n$) and 30 kVA (S_n) is performed, obtaining the active and reactive power output for both converters. Maximum $|S_{load}|$ is greater than S_n but production is shared between both PEC.

The obtained result is compared with completely accurate power sharing, obtaining a per unit error for each scenario as shown in (16a) and (16b). Subscript x indicates the PEC, P_x^*

TABLE III
ERROR IN ACTIVE AND REACTIVE POWER SHARING FOR THE THREE TYPES OF DROOPS

		$P/f + Q/V$	$P/V + Q/f$	Complex
$\phi = 0^\circ$	ΔP	0.00 %	14.49 %	14.28 %
	ΔQ	61.34 %	0.00 %	14.28 %
$\phi = 45^\circ$	ΔP	0.00 %	17.95 %	14.30 %
	ΔQ	17.93 %	0.00 %	14.30 %
$\phi = 90^\circ$	ΔP	0.00 %	61.20 %	14.28 %
	ΔQ	14.49 %	0.00 %	14.28 %
Average	ΔP	0.00 %	31.21 %	14.28 %
	ΔQ	31.25 %	0.00 %	14.28 %

and Q_x^* the power production for perfect accuracy, which is considered to be when both converters have the same power output, since both converters have same rated power and droop coefficient. Taking this into account, $\Delta P_1 = \Delta P_2$ and $\Delta Q_1 = \Delta Q_2$, so the subscript can be omitted.

$$\Delta P_x = \left| \frac{P_x - P_x^*}{S_n} \right| \rightarrow P_x^* = \frac{P_1 + P_2}{2} \quad (16a)$$

$$\Delta Q_x = \left| \frac{Q_x - Q_x^*}{S_n} \right| \rightarrow Q_x^* = \frac{Q_1 + Q_2}{2} \quad (16b)$$

A. Comparison of Different Droop Methods

The results are shown in Fig. 15. First row represents $\Delta P(P_{load}, Q_{load}, \phi)$, considering purely resistive (left column, $\phi = 0^\circ$), purely inductive (right column, $\phi = 90^\circ$) or $R/X = 1$ (middle column, $\phi = 45^\circ$). Different colors are used for different droops. Second row is equivalent but for ΔQ .

The results shown in Fig. 15 are summarized in Table III, where the average errors corresponding to each 3D plot are shown. It can be seen that, as expected, $P/f + Q/V$ droop achieves perfect active power sharing, while $P/V + Q/f$ achieves perfect reactive power sharing. However, complex droop achieves significantly better reactive power sharing accuracy if compared with the $P/f + Q/V$ droop, especially for

TABLE IV
ERROR IN VOLTAGE MAGNITUDE AND FREQUENCY FOR THE THREE TYPES OF DROOPS

		$P/f+Q/V$	$P/V+Q/f$	Complex
$\phi = 0^\circ$	ΔV_{av}	1.45 %	1.44 %	1.45 %
	Δf	0.61 %	0.58 %	0.00 %
$\phi = 45^\circ$	ΔV_{av}	1.45 %	1.45 %	1.39 %
	Δf	0.57 %	0.57 %	0.00 %
$\phi = 90^\circ$	ΔV_{av}	1.44 %	1.45 %	1.45 %
	Δf	0.58 %	0.60 %	0.00 %
Average	ΔV_{av}	1.45 %	1.45 %	1.43 %
	Δf	0.59 %	0.58 %	0.00 %

TABLE V
ERROR IN ACTIVE AND REACTIVE POWER SHARING AND VOLTAGE MAGNITUDE FOR PROPOSED COMPLEX DROOP WITH DIFFERENT IMPEDANCE PHASE ANGLE ESTIMATION

		$\phi_{est} = 0^\circ$	$\phi_{est} = 45^\circ$	$\phi_{est} = 90^\circ$
$\phi = 0^\circ$	ΔP	14.28 %	14.73 %	16.09 %
	ΔQ	14.28 %	14.88 %	16.31 %
	ΔV_{av}	1.45 %	1.38 %	1.46 %
$\phi = 45^\circ$	ΔP	14.83 %	14.30 %	14.79 %
	ΔQ	14.79 %	14.30 %	14.83 %
	ΔV_{av}	1.46 %	1.39 %	1.46 %
$\phi = 90^\circ$	ΔP	16.31 %	14.88 %	14.28 %
	ΔQ	16.09 %	14.73 %	14.28 %
	ΔV_{av}	1.46 %	1.38 %	1.45 %
Average	ΔP	15.14 %	14.64 %	15.05 %
	ΔQ	15.05 %	14.64 %	15.14 %
	ΔV_{av}	1.45 %	1.38 %	1.45 %

the resistive case ($P/f + Q/V$ droop is thought for inductive lines). It also achieves significantly better active power sharing accuracy if compared with the $P/V + Q/f$ droop, especially for the inductive case ($P/f + Q/V$ droop is thought for resistive lines).

Same analysis can be performed for the deviation of voltage magnitude and frequency with respect to rated value. ΔV_x and Δf_x can be obtained as shown in (17a) and (17b). Since $f_1 = f_2$ in steady-state, subscript can be omitted. For ΔV , the average value of both PEC voltage output magnitude is considered.

$$\Delta V_x = \left| \frac{V_x - V_n}{V_n} \right| \quad (17a)$$

$$\Delta f_x = \left| \frac{f_x - f_n}{f_n} \right| \quad (17b)$$

The results are summarized in Table IV. The proposed droop presents no frequency deviation, meanwhile voltage magnitude deviation, considering the average of all scenarios, is approximately equal, as expected from the analysis in Section III.

B. Effect of Impedance Phase Angle Estimation Mismatch

Same analysis is applied for cases with estimation errors for the value of ϕ for the proposed complex droop. The results are summarized in Table V, where the frequency deviation is not included because it is always 0. It can be seen that, estimation mismatches worsen the power sharing accuracy (in each row for ΔP and ΔQ the minimum error appears in the column corresponding to $\phi_{est} = \phi$). However, the errors in active power sharing accuracy are clearly smaller than those obtained for

$P/V + Q/f$ droop and shown in Table III. The active power sharing accuracy of $P/V + Q/f$ droop is only better if lines are resistive and $\phi_{est} \neq \phi$. The same comments apply to reactive power sharing with $P/f + Q/V$ and inductive lines.

Voltage deviation is similar for $\phi_{est} = 0^\circ$ and $\phi_{est} = 90^\circ$ and slightly smaller for $\phi_{est} = 45^\circ$. This is due to the way in which the values of P and Q for the load were considered. For example, the maximum value of $|S|$ for the loads is $|S| = \sqrt{2} \cdot S_n$ kVA for $S = (\pm 1 \pm j)S_n$. This corresponds to α values of 45° , 135° , 225° and 315° . As shown in Fig. 3, $\phi_{est} = 45^\circ$ has no voltage deviation for $\alpha = 135^\circ$ and $\alpha = 315^\circ$, compensating the higher deviation of $\alpha = 45^\circ$ and $\alpha = 225^\circ$.

IX. CONCLUSION

This article has shown a new droop strategy taking into account the coupling terms due to non-purely inductive/resistive lines, using the R/X ratio of the line. This Complex-Valued droop does not require to operate with trigonometric functions, using complex formulations and dq -decomposition instead. A secondary control for the proposed droop is presented too. The HIL results have shown the operation of the proposed complex-valued droop, being able to operate at different R/X ratios with a faster response compared $P/f + Q/V$ and $P/V + Q/f$ alternatives. This includes negative R/X ratios considering capacitive virtual output impedances, showing the validity of the proposed method, as well as the $P/V + Q/f$ droop (universal droop).

The power sharing accuracy of the proposed Complex-Valued droop has been compared with the conventional droops, obtaining better performance in terms of active power sharing if compared with the $P/V + Q/f$ droop, although it is worse than the obtained for the $P/f + Q/V$ droop. However, the $P/f + Q/V$ droop overall performance in resistive scenarios, which is the most typical case in distribution levels (typical scenario for microgrids), is clearly the worst one. So, for this scenario, the proposed droop shows some advantages as compared with the $P/V + Q/f$ droop (better active power sharing and no frequency deviation), although it presents worse reactive power sharing.

The effect of mismatches in the impedance phase angle estimation has been analyzed, showing that the proposed droop control is not much affected by these errors for the complete range of R/X values. Secondary control is more affected by these mismatches, but the error is acceptable for the expected range of estimation mismatch.

REFERENCES

- [1] J. Rocabert, A. Luna, F. Blaabjerg, and P. Rodríguez, "Control of power converters in AC microgrids," *IEEE Trans. Power Electron.*, vol. 27, no. 11, pp. 4734–4749, Nov. 2012.
- [2] J. C. Vasquez, J. M. Guerrero, M. Savaghebi, J. Eloy-Garcia, and R. Teodorescu, "Modeling, analysis, and design of stationary-reference-frame droop-controlled parallel three-phase voltage source inverters," *IEEE Trans. Ind. Electron.*, vol. 60, no. 4, pp. 1271–1280, Apr. 2013.
- [3] E. Lenz, D. J. Pagano, A. Ruseler, and M. L. Heldwein, "Two-parameter stability analysis of resistive droop control applied to parallel-connected voltage-source inverters," *IEEE Trans. Emerg. Sel. Topics Power Electron.*, vol. 8, no. 4, pp. 3318–3332, Dec. 2020.

- [4] A. D. Paquette and D. M. Divan, "Virtual impedance current limiting for inverters in microgrids with synchronous generators," *IEEE Trans. Ind. Appl.*, vol. 51, no. 2, pp. 1630–1638, Mar./Apr. 2015.
- [5] K. De Brabandere, B. Bolsens, J. Van den Keybus, A. Woyte, J. Driesen, and R. Belmans, "A voltage and frequency droop control method for parallel inverters," *IEEE Trans. Power Electron.*, vol. 22, no. 4, pp. 1107–1115, Jul. 2007.
- [6] T. Qunais and M. Karimi-Ghartemani, "Systematic modeling of a class of microgrids and its application to impact analysis of cross-coupling droop terms," *IEEE Trans. Energy Convers.*, vol. 34, no. 3, pp. 1632–1643, Sep. 2019.
- [7] Z. Peng et al., "Droop control strategy incorporating coupling compensation and virtual impedance for microgrid application," *IEEE Trans. Energy Convers.*, vol. 34, no. 1, pp. 277–291, Mar. 2019.
- [8] K. Lao, W. Deng, J. Sheng, and N. Dai, "PQ-coupling strategy for droop control in grid-connected capacitive-coupled inverter," *IEEE Access*, vol. 7, pp. 31663–31671, 2019.
- [9] R. Majumder, B. Chaudhuri, A. Ghosh, R. Majumder, G. Ledwich, and F. Zare, "Improvement of stability and load sharing in an autonomous microgrid using supplementary droop control loop," *IEEE Trans. Power Syst.*, vol. 25, no. 2, pp. 796–808, May 2010.
- [10] H. Han, X. Hou, J. Yang, J. Wu, M. Su, and J. M. Guerrero, "Review of power sharing control strategies for islanding operation of AC microgrids," *IEEE Trans. Smart Grid*, vol. 7, no. 1, pp. 200–215, Jan. 2016.
- [11] J. M. Guerrero, M. Chandorkar, T. Lee, and P. C. Loh, "Advanced control architectures for intelligent microgrids—Part I: Decentralized and hierarchical control," *IEEE Trans. Ind. Electron.*, vol. 60, no. 4, pp. 1254–1262, Apr. 2013.
- [12] R. M. Das, S. Chattopadhyay, and M. Palmal, "A d–q voltage droop control method with dynamically phase-shifted phase-locked loop for inverter paralleling without any communication between individual inverters," *IEEE Trans. Ind. Electron.*, vol. 64, no. 6, pp. 4591–4600, Jun. 2017.
- [13] Y. Li and L. Fan, "Stability analysis of two parallel converters with voltage," *IEEE Trans. Power Del.*, vol. 32, no. 6, pp. 2389–2397, Dec. 2017.
- [14] R. M. Imran, S. Wang, and F. M. F. Flaih, "DQ-Voltage droop control and robust secondary restoration with eligibility to operate during communication failure in autonomous microgrid," *IEEE Access*, vol. 7, pp. 6353–6361, 2019.
- [15] C. Gómez-Aleixandre, A. Navarro-Rodríguez, G. Villa, C. Blanco, and P. García, "Adaptive droop controller for a hybrid 375 VDC/48 VDC/400 VAC AC/DC microgrid," *IEEE Trans. Ind. Appl.*, vol. 58, no. 4, pp. 5104–5116, Jul./Aug. 2022.
- [16] C. Gómez-Aleixandre, C. Blanco, A. Suárez-González, A. Navarro-Rodríguez, and P. García, "Analysis of a complex-valued droop method in AC microgrids with complete steady-state frequency compensation using dq-decomposition," in *Proc. IEEE Energy Convers. Congr. Expo.*, 2021, pp. 1122–1127.
- [17] Q.-C. Zhong and Y. Zeng, "Control of inverters via a virtual capacitor to achieve capacitive output impedance," *IEEE Trans. Power Electron.*, vol. 29, no. 10, pp. 5568–5578, Oct. 2014.
- [18] Q.-C. Zhong and Y. Zeng, "Universal droop control of inverters with different types of output impedance," *IEEE Access*, vol. 4, pp. 702–712, 2016.
- [19] Á. Navarro-Rodríguez, P. García, R. Georgious, and J. García, "Adaptive active power sharing techniques for DC and AC voltage control in a hybrid DC/AC microgrid," *IEEE Trans. Ind. Appl.*, vol. 55, no. 2, pp. 1106–1116, Mar./Apr. 2019.
- [20] J. M. Guerrero, L. Hang, and J. Uceda, "Control of distributed uninterruptible power supply systems," *IEEE Trans. Ind. Electron.*, vol. 55, no. 8, pp. 2845–2859, Aug. 2008.
- [21] C. Gómez-Aleixandre, Á. Navarro-Rodríguez, G. Villa, C. Blanco, and P. García, "Sharing control strategies for a hybrid 48 V/375 V/400Vac AC/DC microgrid," in *Proc. IEEE Energy Convers. Congr. Expo.*, 2020, pp. 3900–3907.
- [22] P. García, M. Sumner, Á. Navarro-Rodríguez, J. M. Guerrero, and J. García, "Observer-based pulsed signal injection for grid impedance estimation in three-phase systems," *IEEE Trans. Ind. Electron.*, vol. 65, no. 10, pp. 7888–7899, Oct. 2018.
- [23] A. Suárez, C. Blanco, P. García, Á. Navarro-Rodríguez, and J. M. Cano Rodríguez, "Grid impedance estimator for active multisource AC grids," *IEEE Trans. Smart Grid*, vol. 14, no. 3, pp. 2023–2033, May 2023.



Carlos Gómez-Aleixandre (Member, IEEE) received the B.Sc. degree in electrical engineering and B.Sc. degree in industrial electronic and automatic engineering from the University of Oviedo, Gijón, Spain, in 2015 and 2018, respectively. He received the M.Sc. degree in sustainable transportation and electrical power systems from the University of Oviedo, University of Nottingham, Nottingham, U.K., Sapienza Università di Roma, Rome, Italy, and Instituto Superior de Engenharia de Coimbra, Coimbra, Portugal, in 2017. In March 2023, he received the Ph.D. degree in energy and process control from the University of Oviedo. He has coauthored five IEEE journals and seven IEEE international conference papers. His research interests include microgrids, coordinated control, and modeling and control of islanded and grid-connected converters. Mr. Gómez-Aleixandre was the recipient of Spanish Predoctoral Grant for the formation in university teaching (Formación de Profesorado Universitario) in 2017.



Ángel Navarro-Rodríguez (Member, IEEE) received the B.Sc. degree in telecommunications engineering with honours from the University of Castilla La-Mancha, Ciudad Real, Spain, in 2012, the M.Sc. degree in electrical energy conversion and power systems, and the Ph.D. degree in energy and process control from the University of Oviedo, Oviedo, Spain, in July 2014 and June 2019, respectively, granted by the government of Principado de Asturias. He is a Ph.D. (*Cum Laude*) in energy and process control. Since October 2019, he has been an Assistant Professor with the Department of Electrical, Electronics, Communications, and Systems Engineering, University of Oviedo. From 2016 to 2017, he was a Visitor Researcher with the PEMC Research Group, University of Nottingham, Nottingham, U.K. In 2022 he was a Visitor Researcher with the Chair of Power Electronics, University of Kiel, Kiel, Germany. He has authored and coauthored 13 IEEE journals and more than 20 IEEE conferences. He was the recipient of the Outstanding Young EPE Member Award in 2018 and the University of Oviedo Outstanding Ph.D. Thesis Award in 2020. He has been a part of the LEMUR research group with the University of Oviedo since July 2014. His research interests include microgrids control and modelling, grid-tied converters, energy storage systems, control systems applied to electrical energy conversion, sustainable transportation and electric traction, power quality, renewable energies integration, and grid modernization and smart grids.



Cristian Blanco (Senior Member, IEEE) was born in Leon Spain. He received the B.S. degree in telecommunications engineering and M.S. and Ph.D. degrees in electrical engineering from the University of Oviedo, Gijón, Spain, in 2010, 2011, and 2015, respectively. From September 2012 to February 2013, he was a Ph.D. Guest with Aalborg University, Aalborg, Denmark. From July 2019 to December 2019, he was a Visiting Faculty with The University of British Columbia, Vancouver, BC, Canada. He is currently an Associate Professor with the Department of Electrical, Computer, and Systems Engineering, University of Oviedo. He was the recipient of a Fellowship for the Personnel Research Training Program in 2011 by the Regional Ministry of Education and Science of Asturias. His research interests include modeling and control of islanded and grid-connected converters including storage systems, hybrid AC/DC microgrids, energy management systems, and hybrid power plants with energy storage capabilities. He was the recipient of the IEEE Energy Conversion Congress and Exposition Second Prize Paper Award, in 2013, and the University of Oviedo Outstanding Ph.D. Thesis Award, in 2016. He is a Member of the LEMUR Research Team.



Geber Villa received the B.Sc. degree in electronics and control engineering, M.Sc. degree in electrical energy conversion and power systems, M.Sc. degree in industrial engineering, and Ph.D. degree in energy and process control, from the University of Oviedo, Gijón, Spain, in 2011, 2016, 2017, and 2022, respectively. He is currently the CTO of ENFASYS, a company specialized in energy management systems to facilitate the integration, control and optimization of distributed energy resources from multiple manufacturers in the distribution grid. In 2019, he was a

Visitor Researcher with the PEMC Research Group, University of Nottingham, Nottingham, U.K. He has coauthored several IEEE international conference and journals papers. His research interests include energy management systems, energy storage systems, analysis and control of power converters, and microgrids. Dr. Villa was the recipient of the Spanish National Award for the Outstanding Graduate of the Year in 2014 and 2021 and a Spanish Predoctoral Grant for the formation in university teaching (Formación de Profesorado Universitario) in 2017.



Andrés Suárez received the M.Sc. degree in electrical engineering from the University of Oviedo, Gijón, Spain, in 2011, the M.Sc. degree in wind power systems from Aalborg University, Aalborg, Denmark, in 2012, and the Ph.D. degree in electrical engineering from the University of Oviedo, in 2020. He was a Research Assistant with the University of Oviedo, in 2012 until joining the Smart Grids Department with Iberdrola Ingeniería y Construcción in 2013, as a Research and Development Engineer. In 2015, he joined LEMUR Research Team with the University

of Oviedo, where has been focusing in the field of grid-tied converters and distributed renewable integration until 2022, when became member of the Technical Regulatory Department of EDP España. His research interests include control of grid-tied converters, parameter estimation and microgrids control, and modelling.



Pablo García (Senior Member, IEEE) was born in Asturias, Spain. He received the M.S. and Ph.D. degrees in electrical engineering from the University of Oviedo, Gijón, Spain, in 2001 and 2006 respectively. From 2002 to 2006, he was awarded with a Fellowship for the National Research and Training Program by the Ministry of Science and Technology in Spain. In 2004, he was a Visiting Scholar with the University of Wisconsin-Madison, Madison, WI, USA. In 2013 he was a Visiting Scholar with the University of Nottingham, Nottingham, U.K. He is currently a Full Professor

with the Department of Electrical, Electronics, Communications and Systems Engineering, University of Oviedo. Since 2022, he has been with the Spanish Research Agency as the Manager of international projects in the energy and transport division area. His research interests include control of grid-tied power converters for distributed resources integration and particularly for the control of grid-tied battery energy storage systems, parameter estimation, optimization of distributed resources and digital signal processing for real-time embedded systems. He is the coauthor of near 40 journal papers and 80 conference papers. He has been the Principal Investigator of 50 projects with companies, 1 European H2020, and 4 national funded projects. He is the Co-Founder of the ENFASYS startup, focused on the development of solutions for the integration of energy storage and collaborative self-consumption applications. He was the recipient of the 2005 IEEE Transactions on Industry Applications, Third Place Prize Paper Award, three IEEE Industry Applications Society Conference prize paper awards in 2006, 2010 and 2016, respectively, and one EPE Conference Award in 2018. He is a Member of the LEMUR research group.